3D phase field modeling of recrystallization in a low-carbon steel

Article *in* Modelling and Simulation in Materials Science and Engineering · November 2012

DOI: 10.1088/0965-0393/20/8/085011

2 authors, including:

Benqiang Zhu
University of British Columbia - Vancouver
7 PUBLICATIONS **25** CITATIONS

SEE PROFILE

3D phase field modelling of recrystallization in a low-carbon steel

2012 Modelling Simul. Mater. Sci. Eng. 20 085011

(http://iopscience.iop.org/0965-0393/20/8/085011)

Modelling Simul. Mater. Sci. Eng. **20** (2012) 085011 (17pp) doi:10.1088/0965-0393/20/8/085011

3D phase field modelling of recrystallization in a low-carbon steel

B Zhu[1] **and M Militzer**

The Centre for Metallurgical Process Engineering, The University of British Columbia, 309-6350 Stores Road, Vancouver, BC, V6T1Z4, Canada

E-mail: zhubq@interchange.ubc.ca and matthias.militzer@ubc.ca

Received 20 August 2012, in final form 24 September 2012
Published 15 November 2012
Online at stacks.iop.org/MSMSE/20/085011

Abstract

Intercritical annealing is a critical processing step to manufacture dual-phase (DP) steels. As part of modelling the microstructure evolution in an intercritical-annealing cycle, a 3D multi-phase field model has been employed to simulate recrystallization during heating of a low-carbon steel that is used to produce commercial DP600 grade. The cold-rolled microstructure obtained from metallographic observations is used as the initial structure in the model. The nucleation conditions and the effective interface mobility are employed as adjustable parameters to fit the experimentally measured kinetics of isothermal recrystallization and then applied to non-isothermal recrystallization. The model predictions are in good agreement with experimental data for recrystallization during continuous heating. The model provides realistic recrystallized microstructures as initial conditions for modelling the subsequent formation and decomposition of austenite.

(Some figures may appear in colour only in the online journal)

1. Introduction

Dual-phase (DP) steel is an attractive advanced high-strength steel (AHSS) for the automotive industry because of its combination of high strength and superior formability. Intercritical annealing of cold-rolled strips in hot dip galvanizing lines is a typical industrial process to manufacture DP steel sheets. The starting microstructure used for intercritical annealing is usually a ferritic matrix with some carbon-rich phases, e.g. lamellar pearlite and/or spheroidized cementite, in the cold-rolled state. The steel strips are initially heated to the intercritical region

[1] Author to whom any correspondence should be addressed.

and held for some time to form a mixture of ferrite and austenite and subsequently cooled down to acquire the DP structures by transforming austenite into martensite. The recrystallization of ferrite takes place during the heating stage. Depending on the heating rate, recrystallization of ferrite may or may not be completed before the start of austenite formation. Previous studies [1–4] have indicated that incomplete recrystallization can greatly affect both the kinetics of austenitization and the austenite morphology. Therefore, it is crucial to study the microstructure evolution during recrystallization before investigating its effects on austenite formation.

In past decades, many studies have focused on the recrystallization of commercial steels. Since both nucleation and growth of new grains during recrystallization are primarily affected by the as-deformed microstructure, detailed information on the as-deformed microstructure is essential to rationalize the recrystallization behaviour. In cold-rolled steels, deformation is usually inhomogeneous such that the dislocation density varies spatially in the microstructure. It is generally concluded that the stored energy in cold-rolled steels is dependent on the crystallographic orientation of individual grains [5–7]. Grains with crystallographic orientations close to the γ-fibre generally have higher stored energy than grains with orientations close to the α-fibre due to larger local misorientation between subgrains. Experimental observations have indicated that nucleation of recrystallization is heterogeneous in low-carbon steels, occurring preferentially in grains with γ-fibre orientations [8]. The deformation inhomogeneity also affects the growth of the new grains since the driving pressure for the interface migration is the stored energy.

The kinetics of recrystallization is frequently described by the Johnson–Mehl–Avrami–Kolmogorov (JMAK) model. However, the JMAK approach is phenomenological in nature and unable to depict the details of the microstructure evolution. In contrast, meso-scale models, e.g. phase field model (PFM), cellular automata (CA) and Monte Carlo (MC) methods, provide much more information about both the recrystallization kinetics and the microstructure evolution. In particular, the phase field approach has recently emerged as a versatile tool to describe various meso-scale phenomena in microstructure engineering, e.g. solidification, solid-state transformation, recrystallization and grain growth [9–12]. The PFM is formulated based on irreversible thermodynamics and is therefore much more physically based than other meso-scale methods. It can easily handle time-dependent growth geometries and describe complex microstructure morphologies, which makes it particularly suitable for modelling phase transformations in steels where morphological complexities are common, e.g. austenite formation and bainitic transformation. A number of recrystallization simulations have been carried out with the CA and MC methods [13, 14]. But there are only limited PFM simulations reported on recrystallization [15–17] with two common drawbacks, i.e. the simulations are all two-dimensional which may lead to unrealistic grain morphologies [18], and none is validated with experimental data. Therefore, it is significant to conduct phase field modelling of recrystallization in three-dimensional space and validate the simulations with experimental results.

As part of modelling the microstructure evolution during an entire intercritical-annealing cycle, a three-dimensional multi-PFM is employed in this paper to describe the recrystallization in a commercial low-carbon steel grade. First, the PFM is benchmarked with the JMAK model in terms of the recrystallization kinetics. Further, the effects of non-uniform stored energy and inhomogeneous nucleation on the recrystallization kinetics and grain size distribution are investigated. Finally, the model is used to predict the recrystallization occurring in the low-carbon steel during the continuous heating stage in an intercritical annealing cycle. The nucleation scenario and the effective grain boundary mobility are fitted with experimental results for isothermal recrystallization. The PFM with the determined nucleation and mobility parameters is then applied to non-isothermal conditions.

2. Model

2.1. Basics of the multi-PFM

The multi-PFM developed originally by Steinbach *et al* [19, 20] is employed to describe the microstructure evolution in terms of both recrystallization kinetics and the resulting grain morphologies. The typical feature of the phase field approach is the assumption of a diffuse interface, i.e. the interface has a much larger thickness than the physical thickness. In this approach, each grain is defined by its own phase field variable ϕ_i. Inside grain i, ϕ_i is equal to 1 while it is 0 outside the grain. Within the interface of width η, ϕ_i changes from 0 to 1 continuously. The phase field variable ϕ_i represents the local fraction of each grain which implies that a constraint of $\sum_i \phi_i = 1$ exists. Each grain can be assigned a set of attributes e.g. phase, crystallographic orientation and stored energy. The temporal evolution of each field variable is described by the superposition of pair-wise interaction with its neighbouring grains [19]:

$$\frac{\mathrm{d}\phi_i}{\mathrm{d}t} = \sum_{i \neq j} \mu_{ij} \left\{ \sigma_{ij} \left[(\phi_j \nabla^2 \phi_i - \phi_i \nabla^2 \phi_j) + \frac{\pi^2}{2\eta^2} (\phi_i - \phi_j) \right] + \frac{\pi}{\eta} \sqrt{\phi_i \phi_j} \Delta G_{ij} \right\}, \tag{1}$$

where μ_{ij} and σ_{ij} are the interfacial mobility and interfacial energy between grain i and grain j, and ΔG_{ij} is the driving pressure which, in this study, is the stored energy difference between grains i and j. When the interface is between a deformed grain and a recrystallized grain, the driving pressure ΔG_{ij} is the stored energy in the deformed grain as the stored energy in new grains is approximately zero. When the interface is between two recrystallized grains, ΔG_{ij} is zero and the migration of the grain boundary is only driven by the curvature effect.

2.2. Construction of the starting structure

A modified Voronoi tessellation [21, 22] is used to construct the elongated polycrystalline microstructure. The cold rolling process is taken as plane strain deformation. Also it is assumed that each grain undergoes the same amount of strain that is identical to the macro-strain.

To construct the pearlite/ferrite structure in the studied steel, the pearlite is assumed as a single pseudo-phase since the size of the pearlitic lamellae is too small to be resolved in the current simulation domain. In the algorithm, a fully ferritic microstructure is constructed first and then a specific number of grains are randomly selected as pearlite nodules to have a pearlite volume fraction consistent with the metallographic observation of the cold-rolled material. Figure 1 is a schematic of a cold-rolled ferrite/pearlite microstructure. To simulate recrystallization, stored energy has to be assigned to the deformed microstructure. The input of stored energy will be discussed in section 3.3.

2.3. Nucleation

The nucleation of recrystallization is distinct from phase transformations. Rather than from thermal fluctuation, the embryos of new grains are formed from the substructures, e.g. dislocation cells or subgrains, which are already present in the deformed microstructure. As a result of dislocation annihilation and subgrain growth or coalescence, some subgrains become nuclei after they form high-angle boundaries ($>15^\circ$). However, the details of the nucleation process, e.g. its kinetics, which is greatly related to the as-deformed microstructure and annealing process, remain elusive. So far, there are no robust physical nucleation models for recrystallization to describe the process in a quantitative way.

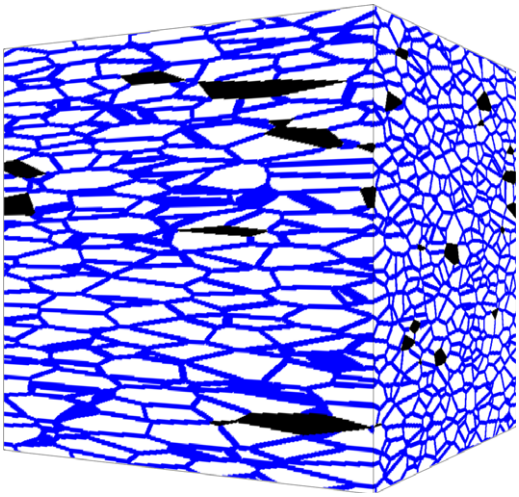

Figure 1. Cold-rolled (50%) ferrite/pearlite microstructure with 5% pearlite (black: pearlite; blue: interface; white: deformed ferrite).

Similar to other meso-scale methods, the phase-field approach is a growth model. A pragmatic way to deal with nucleation is to introduce nuclei as tiny grains into the computational domain explicitly based on a proposed rule that defines nucleation scenarios, e.g. nuclei number and locations. The details of nucleation assumptions in the present approach will be discussed in section 3.2.

2.4. Model parameters and simulation conditions

In this study, isotropic interface properties are assumed, i.e. all grain boundaries have the same interface energy and interface mobility. The grain-boundary energy σ is taken as 0.8 J m^{-2} [23]. The grain-boundary mobility μ in the PFM is an effective mobility implicitly incorporating the potential solute drag effect of alloying elements. It is further assumed that the mobility obeys an Arrhenius relationship

$$\mu = \mu_0 \exp(-Q_{\alpha/\alpha}/RT), \tag{2}$$

where μ_0 is the pre-factor and $Q_{\alpha/\alpha}$ is the activation energy. Here the value of these mobility parameters will be evaluated by fitting the recrystallization kinetics. The similarity between the early recrystallization texture and the final texture in low-carbon steels supports the occurrence of oriented nucleation and opposes selective growth [24]. Since selective growth in steels is usually significant when the material is lightly deformed [24], it is expected that in industrially cold-rolled steels most recrystallization nuclei have grain boundaries of high mobility [25]. Therefore, it is reasonable to assume isotropic interface mobility and energy.

The phase field equations are solved by a finite-difference algorithm in a discrete three-dimensional space. A FORTRAN code parallelized with OpenMP® is developed to solve the phase field equations. The computational domain used in all simulations has a size of $400 \times 400 \times 400$ grid points with periodic boundary conditions. In order to reduce memory cost, a sparse data structure [26] is employed that stores six phase field variables at each grid point since the number of non-zero variables rarely exceeds six at every grid point. The numerical parameters, e.g. the grid spacing Δx, the interface thickness η and the time step

Δt, are carefully chosen such that both satisfactory computational accuracy and efficiency are ensured. In this study the grid spacing is 0.1 μm and the interface thickness is 0.5 μm.

3. Simulation results and discussion

3.1. Benchmark with the JMAK model

The JMAK equation is frequently used to describe recrystallization kinetics. It is strictly derived on the basis of some assumptions and simplifications. Therefore, it is critical to verify the capacity of the PFM to replicate the recrystallization kinetics as described by the JMAK model before it is applied to more complex situations.

In the JMAK model, random nucleation is assumed with either site saturation or constant nucleation rate. Here the case of site saturation is considered. The JMAK model assumes that new grains grow at the same rate in all directions. Accordingly, uniform stored energy and randomly distributed nuclei are assumed in the PFM. Five hundred nuclei are instantaneously put in the simulation domain. The uniform stored energy is 1 MJ m^{-3} and the interface mobility is 1.0 cm^4 J^{-1} s^{-1}, leading to a constant growth rate of 1 μm s^{-1} for the recrystallization fronts.

Figure 2 shows the 3D microstructure evolution of recrystallization under the JMAK assumptions. The new grains grew spherically before they impinge on each other, which replicates the JMAK assumption of isotropic growth. Finally, the new grains completely fill the domain and form equiaxed and polyhedral shapes. Figure 3 shows the JMAK plot of the recrystallization kinetics obtained from the 3D phase field simulation which is a perfectly straight line. The JMAK exponent n is 2.98, which agrees well with the theoretical value of 3. Overall, the PFM has successfully duplicated the recrystallization kinetics depicted by the JMAK equation.

3.2. Effects of inhomogeneity on recrystallization

It is found that the JMAK exponent n when fitted to experimental data is usually much smaller than the theoretical value of 3, which indicates that the assumptions in the JMAK model are unrealistic. Neither random nucleation nor constant growth rate is applicable due to inhomogeneities in the deformed microstructures. Therefore, the effects of the heterogeneities in stored energy and nucleation on recrystallization kinetics are systematically investigated by phase field simulations.

For simplicity, stored energy values between 2 and 6 MJ m^{-3} are randomly generated for each deformed grain to describe the heterogeneity of deformation. To quantitatively simulate the inhomogeneous distribution of nuclei, rather than developing a sophisticated nucleation model, a simple but quantitative model is employed with a minimum number of parameters which stipulates the nucleation mode, nuclei density and nucleation sites. The model assumes site saturation and states that nucleation occurs only in the grains with a stored energy E exceeding a critical value E^*, i.e.

$$E > E^*. \tag{3}$$

Three simulations have been carried out with different nucleation scenarios in the same heterogeneously deformed microstructure (50% cold-rolled microstructure with 50 grains in the domain): the first one assumes homogeneous nucleation (case 1); the other two assume inhomogeneous nucleation with the values of E^* equal to 4 MJ m^{-3} (case 2) and 5 MJ m^{-3} (case 3), respectively. An additional simulation (case 4) is carried out to study the effect of initial grain morphology, i.e. elongation of grains, on recrystallization. The initial microstructure also contains 50 grains but is 90% cold-rolled, resulting in an average aspect ratio of deformed

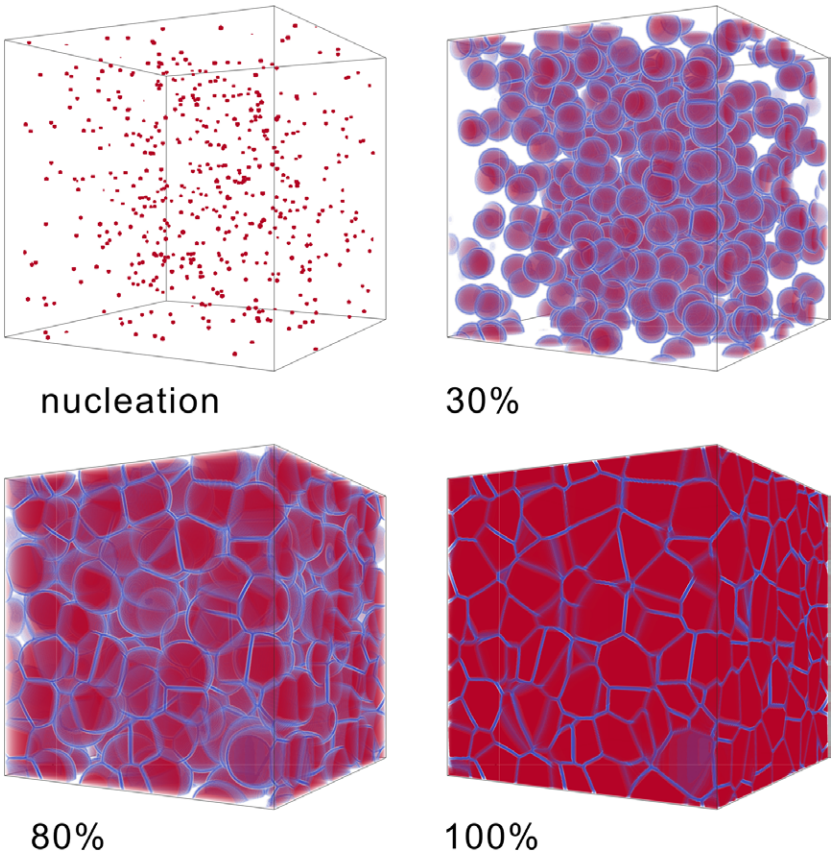

Figure 2. 3D microstructure evolution (nucleation, 30%, 80% and 100% of recrystallization) in the case of homogeneous nucleation and uniform growth rate (blue: interface; red: recrystallized grains).

grains equal to 100 compared with an aspect ratio of 4 for the 50% cold-rolled microstructure. The other parameters, e.g. nucleation parameters are the same as case 3. The nuclei number is in all cases 500.

If the stored energy is varied among grains, the growth rates of the recrystallization fronts are no longer identical and constant. The minimum migration rate can be as low as one third of the maximum corresponding to the range of stored energy, i.e. the assumption of constant growth rate no longer applies. However, the change of the JMAK exponent is modest if the nuclei are randomly distributed (Case 1), only decreasing from 3 to 2.85 (figure 4). This is consistent with the results in the literature [27] that the distribution of growth rates has little effect on the JMAK exponent of the recrystallization kinetics. The final grain size distribution (figure 5(*b*)) also changes little in comparison with the case of uniform stored energy (figure 5(*a*)).

In contrast, the recrystallization kinetics change greatly if the nuclei are located only in some specific grains. The nucleation parameter E^* significantly affects the JMAK exponent which can be as low as 1.7 in the present simulations (case 3). It is evident that greater values of E^* result in smaller n. The interpretation is that the severely clustered nucleation corresponding to high E^* leads to early impingement of grains, slowing down recrystallization.

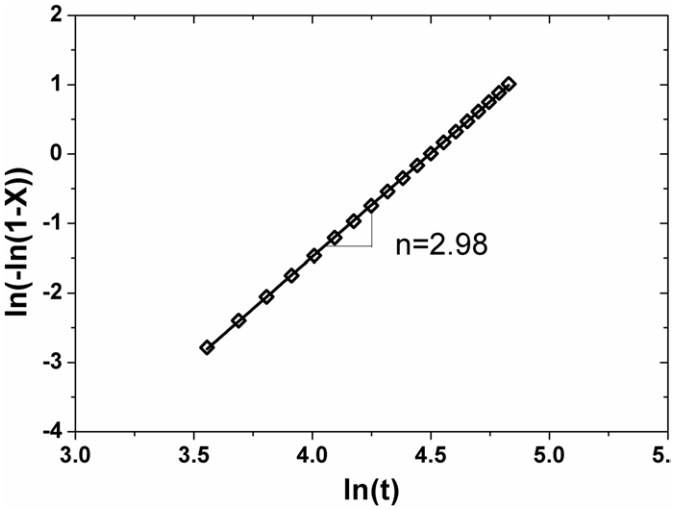

Figure 3. JMAK plots of the simulated recrystallization kinetics: uniform stored energy and homogeneous nucleation.

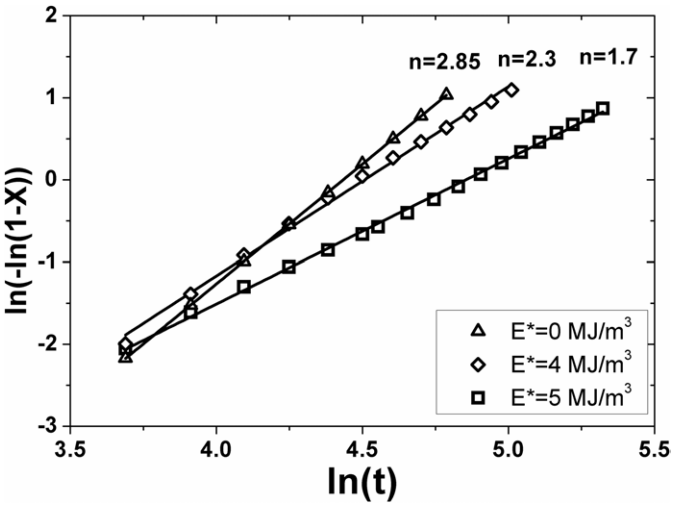

Figure 4. JMAK plots of the simulated recrystallization kinetics: heterogeneous stored energy with various nucleation scenarios.

Moreover, since the nuclei are located in the grains with high stored energy, the migration rates of the recrystallization fronts will decrease with time as they move gradually from areas of high stored energy to areas of low stored energy. Luo *et al* [28] derived the JMAK exponent given by $n = 3(1-r)$ if the decreasing migration rate v is described by $v = C \cdot t^{-r}$. Therefore, it is the clustering of nuclei in the high-stored-energy regions and the subsequently decreasing interface migration rates that cooperatively slow down recrystallization with time and, as a result, reduce the value of the JMAK exponent. Moreover, due to inhomogeneous nucleation, early impingement inhibits the growth of nuclei in the clusters and meanwhile facilitates the growth of nuclei outside the clusters resulting in a wider final grain size distribution, e.g. the maximum size is more than double the average size (figures 5(*c*) and (*d*)).

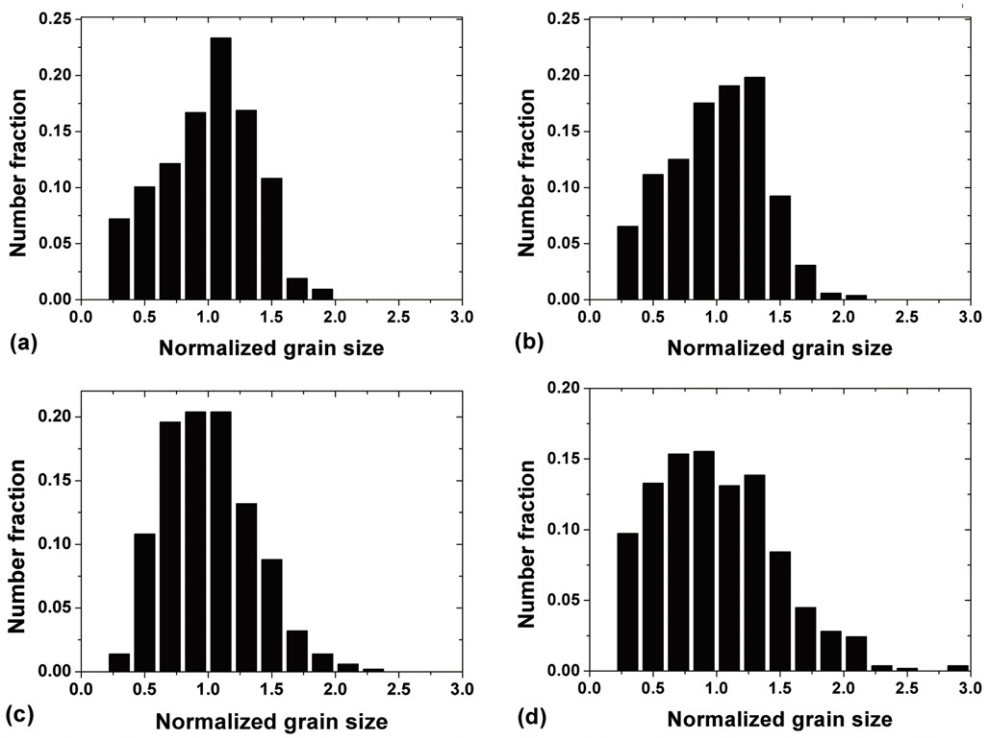

Figure 5. Final grain size distributions: (*a*) uniform stored energy and homogeneous nucleation, (*b*) heterogeneous stored energy and homogeneous nucleation, (*c*), (*d*) heterogeneous nucleation with the critical stored energy of 4 MPa and 5 MPa, respectively.

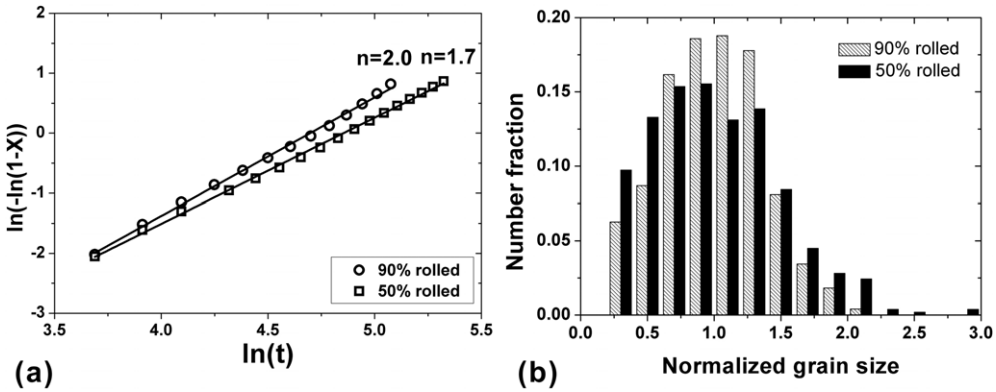

Figure 6. Effect of deformed microstructure morphology on recrystallization: (*a*) JMAK plots and (*b*) final grain size distribution.

As shown in figure 6(*a*), the recrystallization rate is faster and the JMAK exponent is greater in case 4 (90% cold-rolled) than in case 3 (50% cold-rolled) which is consistent with previous studies in the literature [29]. The final grain size distribution also becomes more concentrated around the mean size (figure 6(*b*)). The reason is that more severely elongated grains after larger deformation make the distribution of nuclei less clustered. After 90%

reduction, the polycrystalline microstructure becomes similar to a lamellar structure, where recrystallization nuclei are distributed in layers and early impingement occurs mostly in 2D resulting in faster recrystallization rates and a greater JMAK exponent than in the case of 50% reduction where impingement of nuclei is more pronounced.

In summary, it can be concluded that clustered nucleation in grains of high stored energy is the predominant cause of small values of the JMAK exponent. However, a more elongated grain morphology can lead to larger values of the JMAK exponent.

3.3. Application to intercritical annealing cycle

Three-dimensional phase field calculations were performed to describe the recrystallization occurring in a 50% cold-rolled low-carbon steel (Fe–0.11 wt%C–1.86 wt%Mn–0.16 wt%Si–0.34 wt%Cr) that is used to manufacture DP 600 steel [30]. The microstructure consists of 5% pearlite in a ferrite–bainite matrix that can be approximated as ferrite with an average grain size of 2.8 μm. Experimental data are available for isothermal recrystallization at three temperatures, i.e. 600, 625 and 650 °C, as well as for recrystallization during continuous heating at 1 and 10 °C s^{-1}. The volume fraction of recrystallized ferrite is used to characterize the recrystallization kinetics. The final grain sizes of ferrite after full recrystallization were measured to be approximately 5.0 μm for all investigated isothermal and continuous heating cases.

As described above, pearlite is constructed as a pseudo-phase neglecting the lamellar structure. Spheroidization of cementite, recovery and/or recrystallization of ferrite in pearlite may take place; however, it is quite a challenge to incorporate all these complex phenomena in the PFM. Therefore, it is simplified that the model only takes recrystallization of ferrite into account whereas pearlite is assumed to be an inert phase, i.e. no evolution or interaction with adjacent ferrite grains. This assumption generally has a negligible impact on the overall recrystallization since there is only 5% pearlite in the microstructure. The number of grains used to construct the initial microstructure is selected such that a grain size of 2.8 μm is obtained.

The stored energy distribution can be very complex in a deformed microstructure, i.e. the stored energy varies from grain to grain but can also vary within a grain. In the present case, the recrystallized microstructure is much coarser than the initial microstructure. Then, the overall growth of a new recrystallized grain is expected to be little affected by potential short-range intragranular fluctuations of stored energy. Thus, for simplicity, only stored energy variations from grain to grain are considered here. In detail, a Taylor factor analysis is employed to calculate the stored energy distribution in the cold-rolled pearlite/ferrite steel. Experimental studies [6, 31, 32] have demonstrated that in low-carbon steels the stored energy in a deformed grain increases roughly with the magnitude of the Taylor factor that is associated with its crystallographic orientation. Therefore, as a first approximation, it is assumed that the stored energy in a grain with a specific crystallographic orientation g is proportional to the Taylor factor, i.e.

$$E(g) \propto M(g). \tag{4}$$

According to the Taylor theory, the Taylor factor M is defined as [33]

$$M = \frac{\sum_l \mathrm{d}\gamma_l}{d\varepsilon}, \tag{5}$$

where $\mathrm{d}\varepsilon$ is the incremental macroscopic strain and $\mathrm{d}\gamma_l$ is the absolute value of shear strain contributed by a specific slip system. The value of the Taylor factor for each grain is a function of its crystallographic orientation. The calculation of the Taylor factor can be found

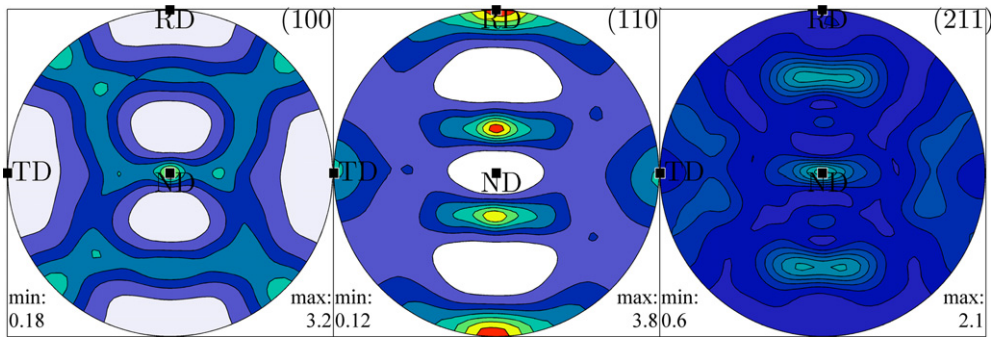

Figure 7. Pole figures of the cold-rolled sample as obtained by x-ray diffraction.

elsewhere [34]. Since each grain has approximately one specific crystallographic orientation in spite of some orientation gradients in the deformed grains, this method proposes that the stored energy is homogeneous within each grain.

In order to obtain the volumetric distribution of the Taylor factor, the distribution of the crystallographic orientation has to be determined. The distribution of crystallographic orientation or the orientation distribution function (ODF) is calculated by the MATLAB® toolbox MTEX [35] with input of the pole figures of the cold-rolled material, which was measured by x-ray diffraction in the present case (figure 7).

Since the stored energy is proportional to the Taylor factor, it has the same distribution as the Taylor factor except that it has to be rescaled by the average stored energy. The average stored energy is estimated with the macroscopic mechanical property of the steel. The average dislocation density ρ_{avg} in the as-deformed steel can be calculated with the difference in the yield stress before and after deformation $\Delta\sigma_{\text{y}}$ given by

$$\Delta\sigma_{\text{y}} = \alpha M_{\text{avg}} G b \sqrt{\rho_{\text{avg}}}, \tag{6}$$

where α is a constant of approximately 0.15; M_{avg} is the average Taylor factor, equal to approximately 3.1 for body-centered-cubic ferrite; G is the shear modulus, equal to 80 GPa; b is the magnitude of Burger's vector, equal to 0.248 nm. The yield stresses before and after cold rolling are 490 MPa and 900 MPa, respectively, which were measured in uniaxial tensile tests. Then an average dislocation density ρ_{avg} of 1700 μm^{-2} is obtained using equation (6). The average stored energy E_{avg} is calculated to be 4.2 MJ m^{-3} according to

$$E_{\text{avg}} = 0.5 G b^2 \rho_{\text{avg}}. \tag{7}$$

The calculated distribution of stored energy is shown figure 8. It can be seen that the maximum stored energy is 5.8 MJ m^{-3}, more than twice of the minimum which is 2.7 MJ m^{-3}.

For nucleation, the model as defined by equation (3) will be used. This model phenomenologically describes the nucleation of recrystallization in both low-carbon and interstitial-free (IF) steels occurring preferentially in γ-fibre grains which store a high density of dislocations [7, 8]. The number of nuclei in the domain is estimated on the basis of the final grain size after full recrystallization. The critical stored energy E^* in the nucleation is an adjustable parameter to fit the recrystallization kinetics.

First, simulations of isothermal recrystallization were carried out for three temperatures to determine the adjustable parameters, i.e. the nuclei number in the domain N, the nucleation parameter E^* and the interface mobility μ. The number of nuclei in the domain is adjusted to obtain the experimentally measured final grain size that is 5.0 μm which is independent of temperature. Further, the JMAK exponents to describe the recrystallization kinetics are

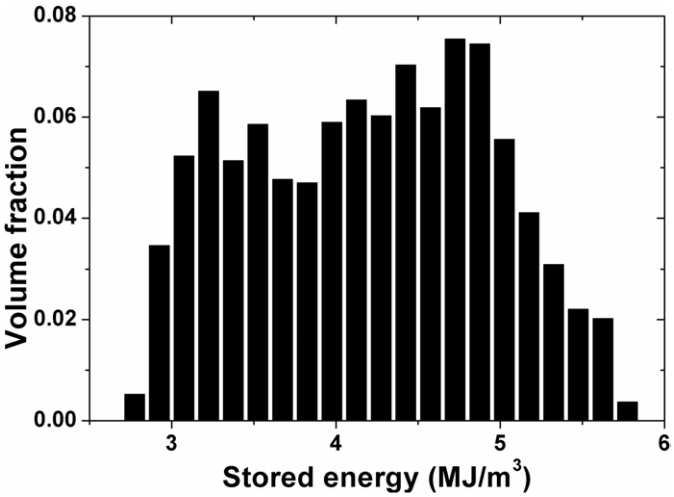

Figure 8. Distribution of stored energy in the cold-rolled microstructure.

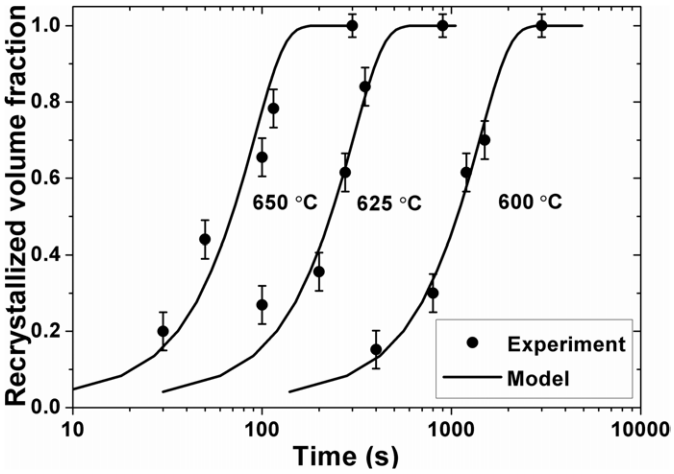

Figure 9. Comparison of calculated recrystallization kinetics with experimental data for various isothermal tests.

approximately equal to 1.5 for all temperatures [30]. The fact that the final grain sizes and the fitted values of the JMAK exponent are approximately the same for all three different temperatures indicates that temperature has a negligible influence on nucleation parameters such that nuclei number N and the critical stored energy E^* are kept temperature-independent. The effective mobility, however, remains a temperature-dependent adjustable parameter.

Good agreement has been reached between the recrystallization kinetics of simulations and experiments by choosing appropriate values of the critical stored energy E^* and interface mobility μ (figure 9). The fitted values of the nucleation parameter E^* and the effective mobility μ for the three temperatures are summarized in table 1. Based on the values of mobility and the estimated stored energy, the migration rates of the recrystallization fronts can be calculated. It is found that the migration rate of the recrystallization fronts at 650 °C is about 28–58 nm s^{-1} while it is only 1.8–3.7 nm s^{-1} at 600 °C. The values of mobility at three

Table 1. Values of fitting parameters.

Temperature (°C)	600	625	650
Nuclei number N in the domain of 40^3 μm^3	400	400	400
Nucleation parameter E^* (10^6 J m^{-3})	5.4	5.4	5.4
Mobility (m^4 J^{-1} s^{-1})	6.3e − 16	3.1e − 15	1.0e − 14

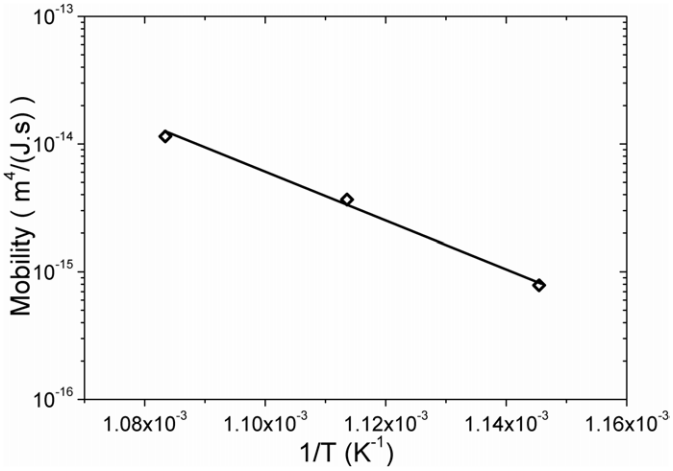

Figure 10. Arrhenius plot of the effective mobility for ferrite grain boundaries.

temperatures are further used to fit the values of the pre-factor μ_0 and the activation energy $Q_{\alpha/\alpha}$. A good fit of the Arrhenius relationship is achieved (figure 10). The pre-factor and the activation energy of mobility are 2.2×10^6 m^4 J^{-1} s^{-1} and 360 kJ mol^{-1}, respectively. The activation energy of the effective mobility is much higher than that of the self-diffusion in pure iron, i.e. 250 kJ mol^{-1} [36], which is probably due to the solute drag effect of the alloying elements, e.g. manganese. Furthermore, the final grain size distribution is compared with the experiments and good agreement is achieved (figure 11). The final grain size basically follows a lognormal distribution with the maximum grain size three times of the average value which also reflects the severe heterogeneity of nucleation in the material.

The 2D cuts of the microstructure in the simulation compare favourably with the experimental micrographs (figure 12) except for the fact that in the experiments fractured cementite lamellas in pearlite and/or bainite have spheroidized and some cementite particles probably located at prior ferrite boundaries are dispersed in the recrystallized ferritic matrix while in the simulations the pearlite remains with its elongated morphology. Because the PFM employs a diffuse interface, there are some artefacts in the 2D cuts, e.g. extended grain boundaries are displayed when the grain boundaries are approximately parallel to the 2D-cut plane.

After the adjustable parameters in the model had been determined from isothermal recrystallization data, simulations for non-isothermal conditions were carried out to validate the model. Two heating rates were used in the simulations of heating tests, i.e. 1 and 10 °C s^{-1}, which are typically employed in intercritical annealing cycles. The simulation starts from 600 °C and ends at 730 °C at which austenite starts to form in the studied steel [30]. The same mobility and nucleation scenario as determined from the isothermal tests are adopted in modelling recrystallization during continuous heating. The simulation results show that

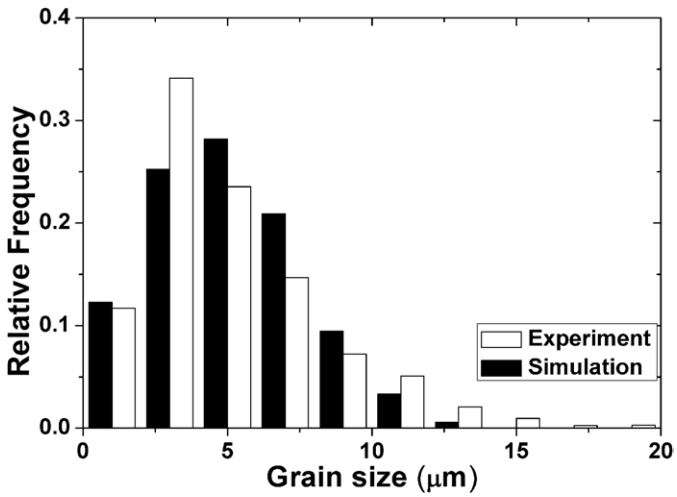

Figure 11. Comparison of calculated final grain size distribution with experimental data for isothermal recrystallization at 650 °C.

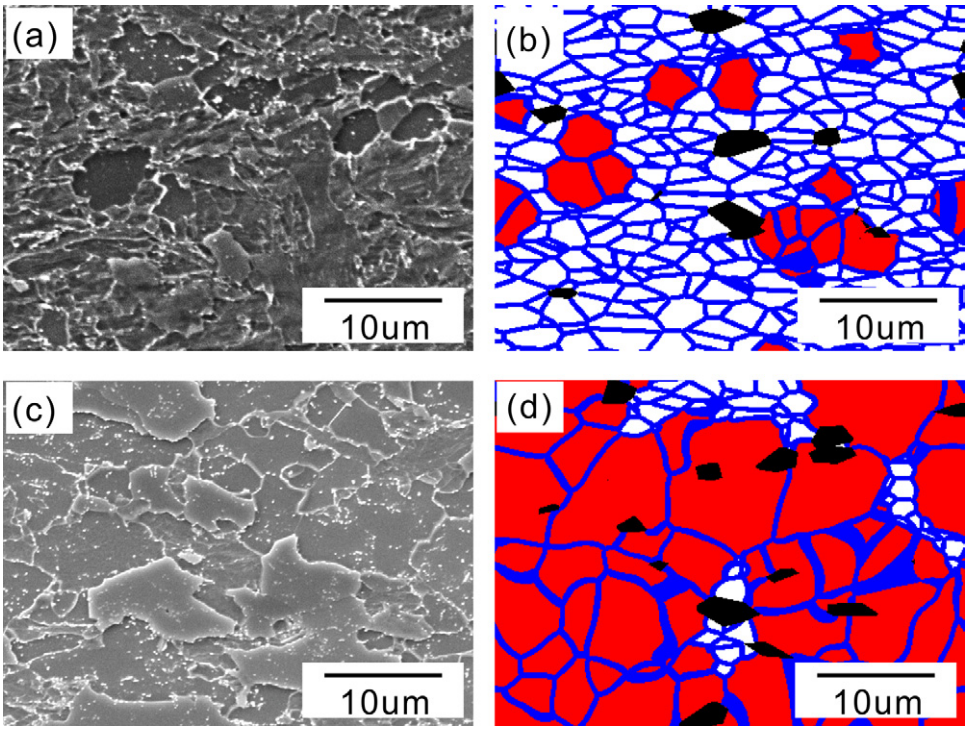

Figure 12. Comparison of predicted microstructures with experimental micrographs of recrystallization at 650 °C with recrystallized volume fraction of (*a*),(*b*) 0.2; (*c*),(*d*) 0.8 (black: pearlite; white: deformed ferrite; red: recrystallized ferrite; blue: interface).

the recrystallization kinetics are in good agreement with the experimentally measured data (figure 13). In the case of heating at 1 °C s^{-1}, the recrystallization reaches a measureable level (∼10%) at approximately 650 °C and finishes around 700 °C below the austenite start temperature. Figure 14 shows the 3D microstructure evolution of recrystallization, which

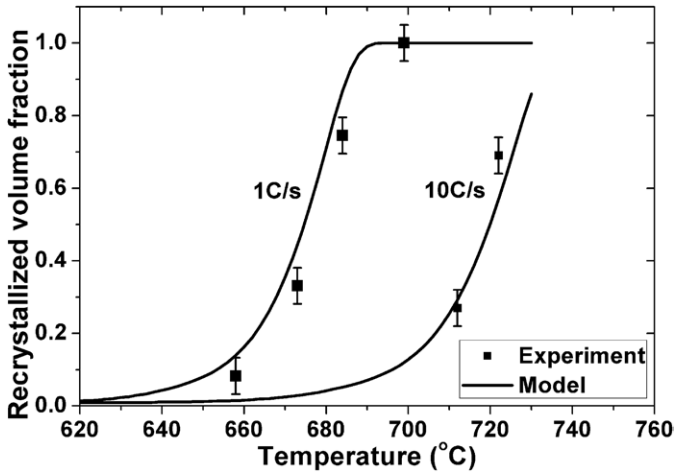

Figure 13. Experimental and predicted recrystallization kinetics for continuous heating.

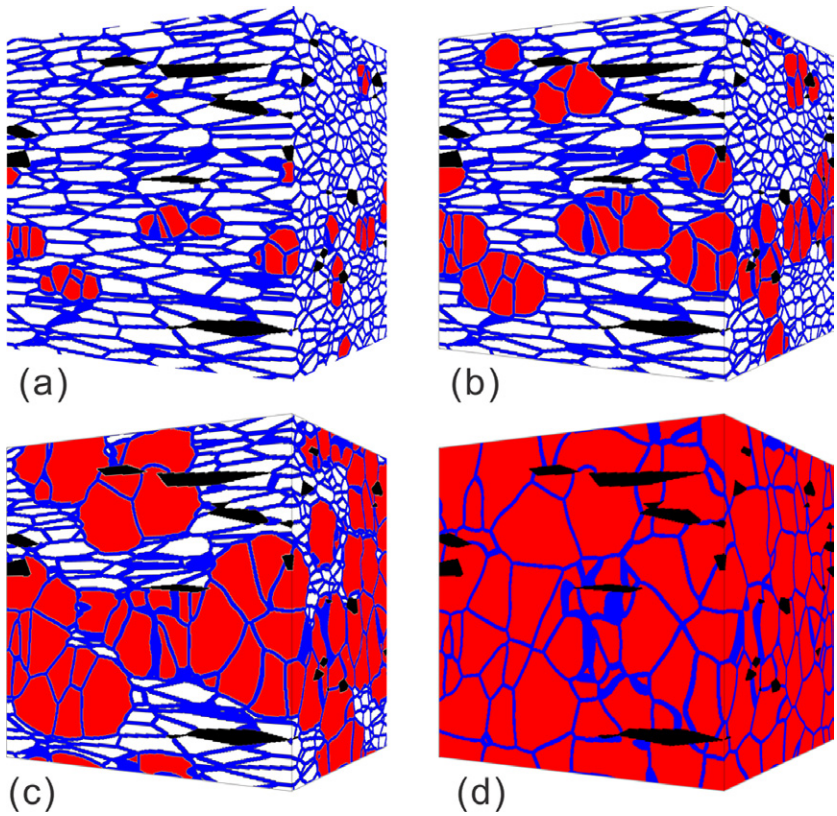

Figure 14. Predicted 3D microstructures for continuous heating at 1 °C s^{-1}: (*a*) 660 °C, (*b*) 670 °C, (*c*) 680 °C and (*d*) 700 °C (black: pearlite; white: deformed ferrite; red: recrystallized ferrite; blue: interface).

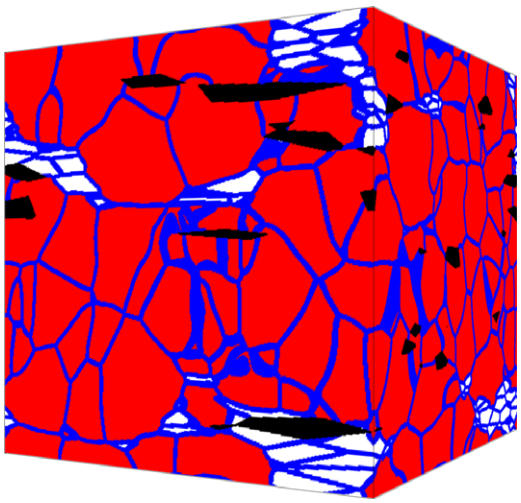

Figure 15. Predicted 3D microstructure at 730 °C for continuous heating at 10 °C s^{-1} (black: pearlite; white: deformed ferrite; red: recrystallized ferrite; blue: interface).

provides very realistic images of microstructures. In the case of heating at 10 °C s^{-1}, the start of recrystallization is delayed to 690 °C and the fraction recrystallized reaches 0.85 at the austenite start temperature of 730 °C (figure 15), i.e. for such a heating rate austenite would start to form from a partially recrystallized microstructure. Furthermore, it is notable that during recrystallization, some new grains have disappeared due to grain growth.

4. Conclusions

A 3D multi-PFM has been employed to simulate recrystallization. The kinetics predicted by the JMAK theory can be accurately duplicated by the PFM. Based on the study of inhomogeneous deformation and nucleation, it can be concluded that the inhomogeneity of nucleation for recrystallization is the main reason that leads to the lower JMAK exponents (<3) typically observed in experiments. With input of experimental data, e.g. initial microstructure, mean stored energy and nuclei density, reliable values of physical parameters, e.g. grain boundary mobility, can be obtained from phase field simulations. The accurate prediction of the recrystallization kinetics during continuous heating using the model parameters as derived from isothermal recrystallization confirms the additive nature of recrystallization.

Overall, the PFM can reliably provide partially or completely recrystallized microstructures as the starting structures for austenite formation in an intercritical-annealing cycle. In the future, a PFM for austenite formation will be developed and integrated with the recrystallization model to describe the potentially concurrent recrystallization and austenitization during intercritical annealing.

Acknowledgments

The authors are grateful to the Natural Sciences and Engineering Research Council of Canada (NSERC) and ArcelorMittal Dofasco Inc. for their financial support. Discussions with Professor Warren Poole are also greatly appreciated. Further, the authors thank Mykola Kulakov for providing experimental data for recrystallization and Guillaume Lefebvre for conducting the x-ray diffraction measurement.

References

[1] Azizi-Alizamini H and Militzer M 2010 Phase field modelling of austenite formation from ultrafine ferrite-carbide aggregates in Fe–C *Int. J. Mater. Res.* **101** 534–41

[2] Huang J, Poole W J and Militzer M 2004 Austenite formation during intercritical annealing *Metall. Mater. Trans.* A **35A** 3363–75

[3] Ogawa T, Maruyama N, Sugiura N and Yoshinaga N 2010 Incomplete Recrystallization and subsequent microstructural evolution during intercritical annealing in cold-rolled low carbon steels *ISIJ Int.* **50** 469–75

[4] Yang D Z, Brown E L, Matlock D K and Krauss G 1985 The formation of austenite at low intercritical annealing temperatures in a normalized 0.08C-1.45Mn-0.21Si steel *Metall. Trans.* A **16** 1523–6

[5] Bacroix B, Miroux A and Castelnau O 1999 Simulation of the orientation dependence of stored energy during rolling deformation of low carbon steels *Modelling Simul. Mater. Sci.* **7** 851–64

[6] Castro S F, Gallego J, Landgraf F J G and Kestenbach H J 2006 Orientation dependence of stored energy of cold work in semi-processed electrical steels after temper rolling *Mater Sci. Eng.* A **427** 301–5

[7] Samet-Meziou A, Etter A L, Baudin T and Penelle R 2008 Relation between the deformation sub-structure after rolling or tension and the recrystallization mechanisms of an IF steel *Mater. Sci. Eng.* A **473** 342–54

[8] Oyarzabal M, Martinez-De-Guerenu A and Gutierrez I 2008 Effect of stored energy and recovery on the overall recrystallization kinetics of a cold rolled low carbon steel *Mater. Sci. Eng.* A **485** 200–9

[9] Bottger B, Eiken J and Steinbach I 2006 Phase field simulation of equiaxed solidification in technical alloys *Acta Mater.* **54** 2697–704

[10] Militzer M and Azizi-Alizamini H 2011 Phase field modelling of austenite formation in low carbon steels *Solid State Phenom.* **172–174** 1050–9

[11] Toloui M and Militzer M 2010 Phase field simulation of austenite grain growth in the HAZ of microalloyed linepipe steel *Int. J. Mater. Res.* **101** 542–8

[12] Warren J A, Kobayashi R, Lobovsky A E and Carter W C 2003 Extending phase field models of solidification to polycrystalline materials *Acta Mater.* **51** 6035–58

[13] Doherty R D, Hughes D A, Humphreys F J, Jonas J J, Jensen D J, Kassner M E, King W E, McNelley T R, McQueen H J and Rollett A D 1997 Current issues in recrystallization: a review *Mater. Sci. Eng.* A **238** 219–74

[14] Raabe D 2007 Multiscale recrystallization models for the prediction of crystallographic textures with respect to process simulation *J. Strain Anal. Eng.* **42** 253–68

[15] Jou H J and Lusk M T 1997 Comparison of Johnson-Mehl-Avrami-Kologoromov kinetics with a phase-field model for microstructural evolution driven by substructure energy *Phys. Rev.* B **55** 8114–21

[16] Suwa Y, Saito Y and Onodera H 2008 Phase-field simulation of recrystallization based on the unified subgrain growth theory *Comput. Mater. Sci.* **44** 286–95

[17] Takaki T, Yamanaka A, Higa Y and Tomita Y 2007 Phase-field model during static recrystallization based on crystal-plasticity theory *J. Comput.-Aided Mater.* **14** 75–84

[18] Militzer M, Mecozzi M G, Sietsma J and van der Zwaag S 2006 Three-dimensional phase field modelling of the austenite-to-ferrite transformation *Acta Mater.* **54** 3961–72

[19] Eiken J, Bottger B and Steinbach I 2006 Multiphase-field approach for multicomponent alloys with extrapolation scheme for numerical application *Phys. Rev.* E **73** 066122

[20] Steinbach I and Pezzolla F 1999 A generalized field method for multiphase transformations using interface fields *Physica* D **134** 385–93

[21] Fritzen F, Bohlke T and Schnack E 2009 Periodic three-dimensional mesh generation for crystalline aggregates based on Voronoi tessellations *Comput. Mech.* **43** 701–13

[22] Seo Y S, Chun Y B and Hwang S K 2008 A 3D Monte-Carlo simulation study of recrystallization kinetics in Zr with hypothetical stored energy gradients *Comput. Mater. Sci.* **43** 512–21

[23] Raabe D and Hantcherli L 2005 2D cellular automaton simulation of the recrystallization texture of an IF sheet steel under consideration of Zener pinning *Comput. Mater. Sci.* **34** 299–313

[24] Sanchez-Araiza M, Godet S, Jacques P J and Jonas J J 2006 Texture evolution during the recrystallization of a warm-rolled low-carbon steel *Acta Mater.* **54** 3085–93

[25] Cao S Q, Li Y Y, Zhang J X and Wu J S 2007 EBSD investigation on oriented nucleation in IF steels *J. Mater. Sci. Technol.* **23** 262–6

[26] Kim S G, Kim D I, Kim W T and Park Y B 2006 Computer simulations of two-dimensional and three-dimensional ideal grain growth *Phys. Rev.* E **74** 061605

[27] Godiksen R B, Schmidt S and Jensen D J 2007 Effects of distributions of growth rates on recrystallization kinetics and microstructure *Scr. Mater.* **57** 345–8

[28] Luo H W, Sietsma J and van der Zwaag S 2004 Effect of inhomogeneous deformation on the recrystallization kinetics of deformed metals *ISIJ Int.* **44** 1931–6

[29] Kugler G and Turk R 2006 Study of the influence of initial microstructure topology on the kinetics of static recrystallization using a cellular automata model *Comut. Mater. Sci.* **37** 284–91
[30] Kulakov M, Poole W J and Militzer M 2010 Recrystallization and austenite formation during continuous heating of multi-phase steel *Mater. Sci. Tech. 2010 Conf.* 1316–26
[31] Rajmohan N and Szpunar J A 2000 A new model for recrystallization of heavily cold-rolled aluminum using orientation-dependent stored energy *Acta Mater.* **48** 3327–40
[32] Hutchinson B 1999 Deformation microstructures and textures in steels *Phil. Trans. R. Soc.* A **357** 1471–85
[33] Rosenber J M and Piehler H R 1971 Calculation of Taylor factor and lattice rotations for BCC metals deforming by pencil glide *Metall. Trans.* **2** 257–9
[34] Orlans-Joliet B, Bacroix B, Montheillet F, Driver J H and Jonas J J 1988 Yield surfaces of BCC crystals for slip on the (1 1 0) (1 1 1) and (1 1 2) (1 1 1) systems *Acta Metall. Mater.* **36** 1365–80
[35] Bachmann F, Hielscher R and Schaeben H 2010 Texture analysis with MTEX - free and open source software toolbox *Texture Anisotropy Polycryst: III* **160** 63–8
[36] Kucera J, Million B, Ruzickov J, Foldyna V and Jakobova A 1974 Self-diffusion of iron in alpha-phase of iron and Fe–Cr alloys *Acta Metall. Mater.* **22** 135–40